Chapter 2
Silicon Thyristors

As discussed in the textbook [1], the power thyristor was developed as a replacement for the thyratron, a vacuum tube used for power applications prior to the advent of solid-state devices. The simple construction of these structures using P-N junctions enabled commercialization of devices in the 1950s. These devices were found to be attractive from an applications viewpoint because they eliminated the need for the cumbersome filaments required in vacuum tubes and were much more rugged and smaller in size. The power thyristor provides both forward and reverse voltage blocking capability, making it well suited for AC power circuit applications. The device can be triggered from the forward-blocking off-state to the on-state by using a relatively small gate control current. Once triggered into the on-state, the thyristor remains stable in the on-state even without the gate drive current. In addition, the device automatically switches to the reverse-blocking off-state upon reversal of the voltage in an AC circuit. These features greatly simplify the gate control circuit, relative to that required for the power transistor, reducing its cost and size.

Due to significant interest in the development of solid-state devices for the control of motors operating from DC power sources, a structure called the *gate turn-off thyristor* (abbreviated as GTO), was also developed in the 1960s. In this device, the structure is modified to enable the switching of the device from the on-state to the off-state while operating in the first quadrant. This is performed by the application of a large reverse gate drive current, akin to that used for turning off the bipolar power transistor. In spite of the bulky and expensive gate control circuits required for the GTO, it was widely adopted for the control of motors in traction (electric street-cars and electric locomotives) applications until recently. The scaling of the power handling capability of the insulated gate bipolar transistor (IGBT) to handle very high (megawatt) power levels in the twenty-first century has resulted in the displacement of these devices by the IGBT in traction applications.

B.J. Baliga, *Advanced High Voltage Power Device Concepts*,
DOI 10.1007/978-1-4614-0269-5_2,

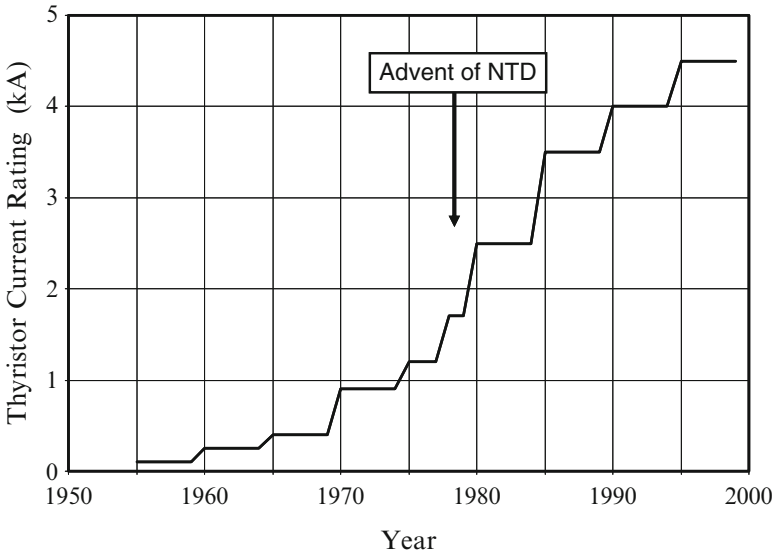

Fig. 2.1 Growth in current ratings for the thyristor

The ability to control operation between the blocking and on states for a thyristor by using a third terminal was first reported in the 1950s [2, 3]. The extensive application potential for these devices to home appliances and power distribution systems generated strong interest in making improvements in the power ratings for the thyristors. The growth of the current handling capability for the power thyristors is charted in Fig. 2.1. Starting with a modest current of 100 A in the 1950s, the current rating has been scaled to approach 5,000 A for a single device. These high current levels are required for power distribution systems, such as high voltage DC transmission (HVDC) networks. From the figure, it can be observed that the most rapid increase in the current handling capability took place at the end of the 1970s. This outcome can be traced to the development of the neutron-transmutation-doping (NTD) process in the mid-1970 time frame. Using the NTD process, it became possible to obtain larger diameter silicon wafers with uniform properties enabling the observed scaling of the current handling capability of thyristors.

There was a concomitant increase in the voltage blocking capability for the thyristor as illustrated in the chart in Fig. 2.2. Beginning with devices capable of operating upto a few hundred volts in the 1950s, the voltage rating for thyristors has been escalated to 8,000 V. The increase in the voltage rating had to be accomplished by the availability of higher resistivity silicon wafers. This was initially achieved by the development of the float-zone process. However, the resistivity variation produced by this process was inadequate for utilization in the large diameter wafers desired to increase the current ratings. The NTD process was instrumental in providing the breakthrough required to create large diameter silicon wafers with low n-type doping concentration and high uniformity in the resistivity across the wafers. Consequently, a substantial gain in the voltage rating

occurred in the late 1970s after the commercial availability of NTD silicon as indicated in the chart.

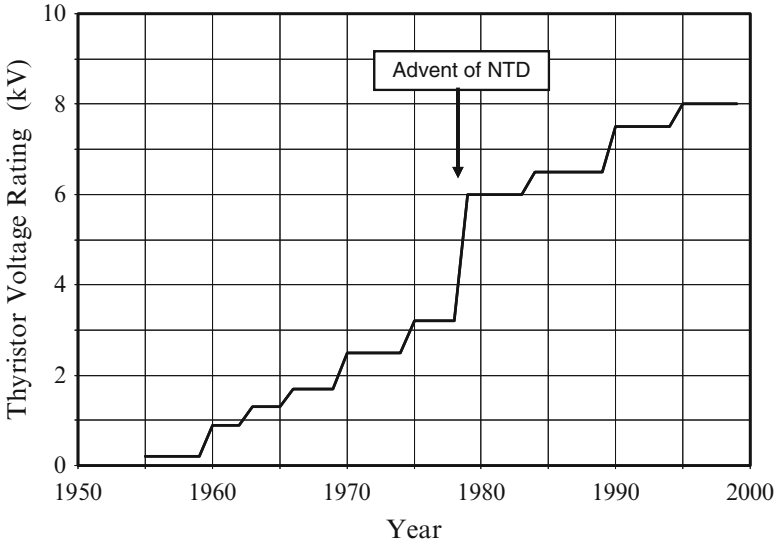

Fig. 2.2 Growth in voltage ratings for the thyristor

Today, single thyristors are available with the capability to block over 8,000 V and conduct 5,000 A in the on-state. Consequently, a single thyristor device can control 40 MW of power. Such devices are attractive for power distribution networks to reduce the total number of devices required in a HVDC station. The reduction in the number of devices connected in series and parallel provides the added benefits of a smaller number of other components that are needed in the system to ensure proper voltage and current distribution between the multiple thyristors. Light-triggered thyristors have also been developed to enable stacking them in a series string to hold off the very high voltages (in excess of 100 kV) that are commonplace for power distribution.

The basic structure and operation of the thyristor were discussed in the textbook. The thyristor contains two coupled bipolar transistors that provide an internal positive feedback mechanism that allows the device to sustain itself in the on-state. This internal feedback mechanism makes it difficult to turn off the structure by external means. In order to enable operation at elevated temperatures, it is necessary to short-circuit the emitter and base regions of the thyristor. The impact of this on the gate control current and switching behavior was also analyzed in the textbook. Analytical models were provided in the textbook for all the operating modes of the thyristor, including the switching transient for the GTO. These models are applicable to the devices with high (>5,000 V) blocking voltage capability discussed in this monograph. The characteristics of high voltage silicon carbide thyristors are also considered in the next chapter for blocking voltage rating of 20 kV because there are no high performance silicon devices available with blocking voltages above 10 kV.

2.1 Power Thyristor Structure and Operation

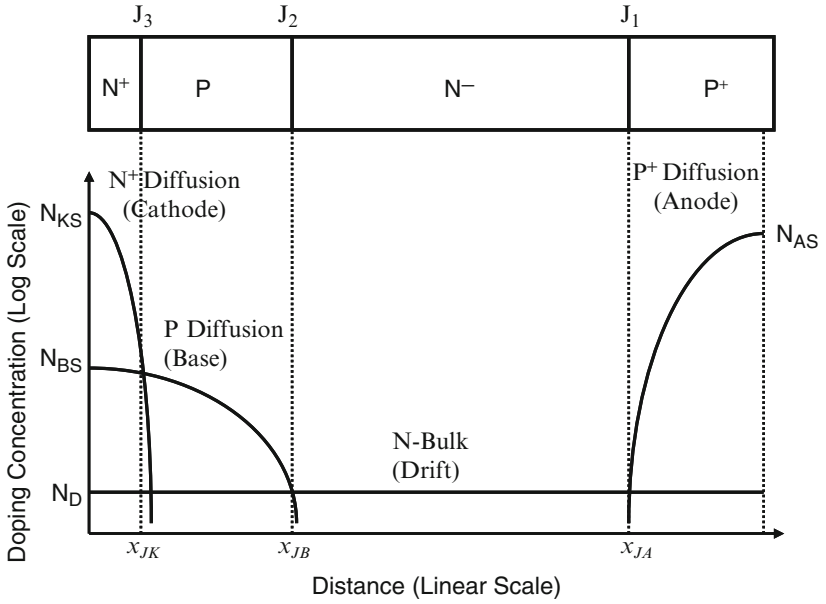

Fig. 2.3 The power thyristor structure and its doping profile

The basic structure for an N^+-P-N-P^+ power thyristor is illustrated in Fig. 2.3. The structure is usually constructed by starting with a lightly doped N-type silicon wafer whose resistivity is chosen based upon the blocking voltage rating for the device. The anode P^+ region is formed by the diffusion of dopants from the backside of the wafer to a junction depth x_{JA}. The P-base and N^+ cathode regions are formed by the diffusion of dopants from the front of the wafer to a depth of x_{JB} and x_{JK}, respectively. Electrodes are formed on the front side of the wafer to contact the cathode and P-base regions, and on the backside of the wafer to contact the anode region. No contact electrode is usually attached to the N-drift (N-base) region.

In order to achieve such high voltage blocking capability in both forward and reverse operating quadrants, the P^+ anode/N-drift junction and the P-base/N-drift junction must have a highly graded doping profile. This increases the blocking voltage capability due to voltage supported on the more highly doped side of the junction and allows the utilization of the positive and negative bevels at the edges to suppress premature breakdown at the junction termination. The highly graded junctions can be produced by using gallium and aluminum as the p-type dopants instead of boron, the more commonly used dopant for integrated circuits as well as other power devices discussed in the book. These dopants have much larger diffusion coefficients than boron, allowing the production of large junction depths (20–100 μm) in a reasonable processing time. Gallium is used as the dopant for the P^+ anode region because of its high solid solubility. Aluminum is used as the dopant for the P-base region due to

its lower solid solubility. The doping concentration for the P-base region of the thyristor must be in the range of $1 \times 10^{16} - 1 \times 10^{17}$ cm^{-3} to obtain a reasonable gain for the internal N-P-N bipolar transistor and for enabling edge termination with a negative bevel for the P-base/N-drift junction.

The output characteristics for the thyristor structure are illustrated in Fig. 2.4. The thyristor structure contains three P-N junctions that are in series as indicated in Fig. 2.3. When a negative bias is applied to the anode terminal of the device, the P^+ anode/N-drift junction (J_1) and the N^+ cathode/P-base junction (J_3) become reverse biased, while the P-base/N-drift junction (J_2) becomes forward biased. Due to high doping concentrations on both sides of the N^+ cathode/P-base junction (J_3), it is capable of supporting less than 50 V. Consequently, most of negative bias applied to the anode terminal is supported by the P^+ anode/N-drift junction (J_1). The reverse blocking voltage capability for the device is determined by the doping concentration and thickness of the N-drift region. Note that an open-base bipolar transistor is formed within the thyristor structure between junctions J_1 and J_2. Consequently, the breakdown voltage is not determined by the avalanche breakdown voltage but by the open-base transistor breakdown voltage. The width of the N-drift region between these two junctions must be carefully optimized to maximize the blocking voltage capability and minimize the on-state voltage drop.

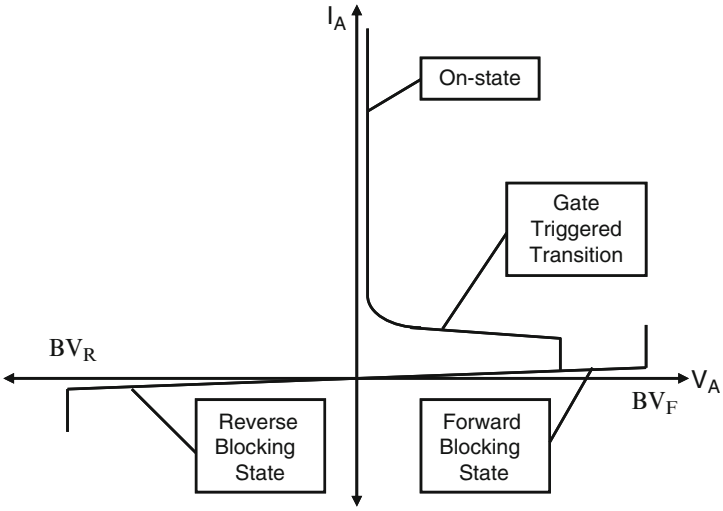

Fig. 2.4 Output characteristics of the power thyristor structure

When a positive bias is applied to the anode terminal of the thyristor, the P^+ anode/N-drift junction (J_1) and the N^+ cathode/P-base junction (J_3) become forward biased while the junction (J_2) between the P-base region and the N-drift region becomes reverse biased. The applied positive bias is mostly supported across the N-drift region. As in the case of reverse blocking operation, the blocking voltage capability is determined by open-base transistor breakdown

rather than avalanche breakdown. The reverse and forward blocking capability for the thyristor structure must be approximately equal, making it suitable for use in AC power circuits. This is achieved by using cathode shorts to reduce the gain of the N-P-N transistor at low leakage current levels. A cross section of the thyristor with the cathode short is illustrated in Fig. 2.5.

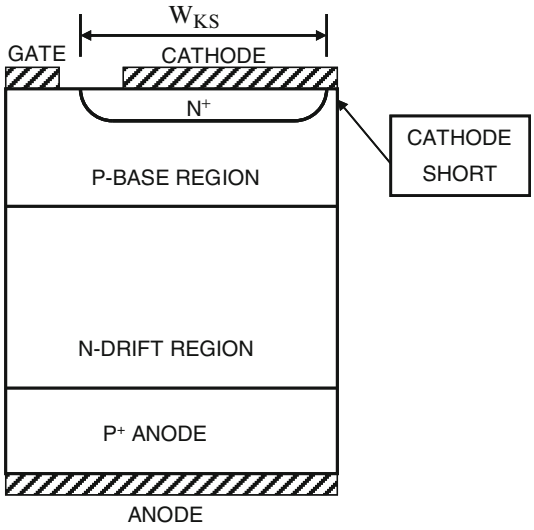

Fig. 2.5 Thyristor structure with cathode short

Current flow through the thyristor can be induced in the first quadrant of operation by using a current supplied through the gate terminal to trigger the device into its on-state. The gate current forward biases the N^+ cathode/P-base junction (J_3) to initiate the injection of electrons. The injected electrons trigger a positive feedback mechanism produced by the two coupled bipolar transistors within the thyristor structure. The first bipolar transistor is an N-P-N transistor formed between the N^+ cathode/P-base/N-drift regions while the second bipolar transistor is a P-N-P transistor formed between the P^+ anode/N-drift/P-base regions. Once current flow is initiated through the transistors, they are able to provide the base drive current for each other by a process referred to as *regenerative action*. In this process, the collector current of the N-P-N transistor provides the base drive current for the P-N-P transistor and the collector current of the P-N-P transistor provides the base drive current for the N-P-N transistor. The regenerative action inherent within the thyristor structure allows stable operation of the device in its on-state without any external gate drive current. This is one of its advantages when compared with the bipolar transistors.

Once the thyristor is operating in its on-state, the *i–v* characteristics can be shown to become similar to that for a P-i-N rectifier, resulting in the anode current increasing exponentially with the on-state voltage drop (or anode–cathode voltage). Consequently, thyristors can be designed with very high voltage blocking capability with low on-state voltage drops making them excellent power devices for circuits used in power distribution systems.

The power thyristor can be switched from its on-state to the blocking state by reversing the bias applied to the anode electrode. The reverse bias applied to the anode electrode forces the thyristor to undergo a reverse-recovery process similar to that observed in a P-i-N rectifier. Once the thyristor has entered the reverse blocking mode, a positive voltage can once again be applied to the anode without turning on the device until a gate control signal is applied.

2.2 5,000-V Silicon Thyristor

The design and characteristics of the 5,000-V symmetric blocking silicon thyristor structure are discussed in this section. The design parameters for the N-base region required to achieve this blocking voltage are first analyzed. Using the optimum N-base width, the blocking characteristics for the device are then obtained as a function of the lifetime in the drift region. The on-state characteristics for the device are obtained for various lifetime values as well. The switching behavior of the thyristor structure is obtained by observation of the turn-on process and the reverse recovery process.

2.2.1 Blocking Characteristics

The physics for blocking voltages in the first and third quadrants by thyristors is discussed in detail in the textbook. The device can have equal or symmetric forward and reverse blocking capability if cathode shorts are utilized to suppress the gain of the N-P-N transistor when small leakage currents are flowing in the structure. The reverse blocking voltage is supported across the P^+ anode/N-drift junction with a depletion layer extending mostly within the N-drift region. The maximum electric field occurs at the P^+ anode/N-drift junction (J_1). The forward blocking voltage is supported across the P-base/N-drift junction, with a depletion layer extending mostly within the N-drift region. The maximum electric field occurs at the P-base/N-drift junction (J_2).

The breakdown voltage for the thyristor in both blocking modes is governed by the open-base transistor breakdown phenomenon [4]. According to open-base-transistor breakdown [1], the anode current will increase very rapidly when the common base current gain of the P-N-P bipolar transistor within the thyristor structure approaches unity. As the anode bias is increased, the width of the un-depleted portion of the N-drift region becomes smaller, producing an increase in the base transport factor (α_T). Concurrently, the maximum electric field at the blocking junction becomes larger leading to an increase in the multiplication coefficient. Both phenomena produce an increase in the common base current gain with increasing anode bias until it becomes equal to unity resulting in open-base transistor breakdown.

The open-base transistor breakdown condition is given by:

$$\alpha_{PNP} = (\gamma_E \cdot \alpha_T)_{PNP} M = 1 \tag{2.1}$$

The injection efficiency of the P-base/N-drift and P^+ anode/N-drift junctions is close to unity because of the relatively high doping concentration in the P^+ anode and P-base regions and the low doping concentration of the N-drift region. The magnitude of the other two terms in the above equation is a function of the anode bias. The base transport factor is determined by the width (l) of the un-depleted portion of the N-drift region:

$$\alpha_T = \frac{1}{\cosh(l/L_P)} \tag{2.2}$$

with

$$l = W_N - \sqrt{\frac{2\varepsilon_S V_A}{qN_D}} \tag{2.3}$$

where V_A is the applied bias to the anode electrode. As the anode bias increases, the width of the un-depleted portion of the N-drift region shrinks resulting in an increase in the base transport factor.

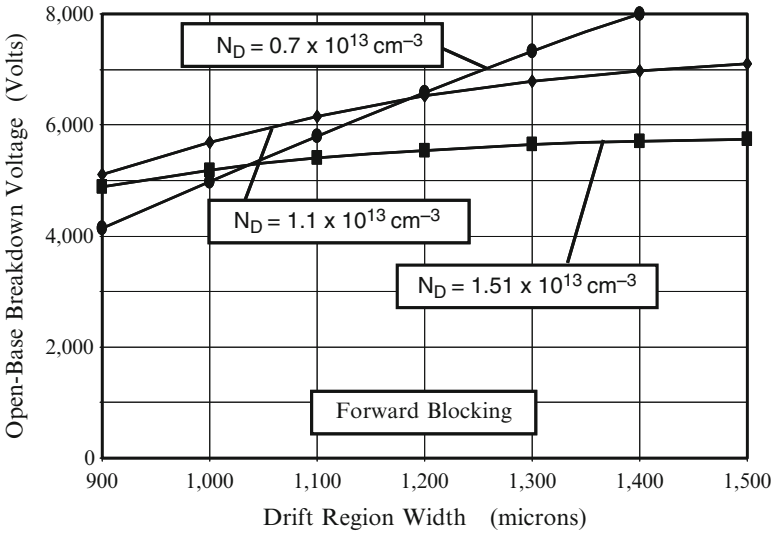

Fig. 2.6 Open-base breakdown voltage for the 5,000-V power thyristor structure

During forward blocking, the multiplication factor is determined by the anode bias relative to the avalanche breakdown voltage of the P-base/N-drift junction ($BV_{PP,F}$):

$$M = \frac{1}{1 - \left(V_A / BV_{PP,F}\right)^n} \tag{2.4}$$

where $n = 6$ for the case of a P^+/N diode. The multiplication coefficient also increases with increasing anode bias. The open-base transistor breakdown voltage is determined by the anode voltage at which the multiplication factor becomes equal to the reciprocal of the base transport factor.

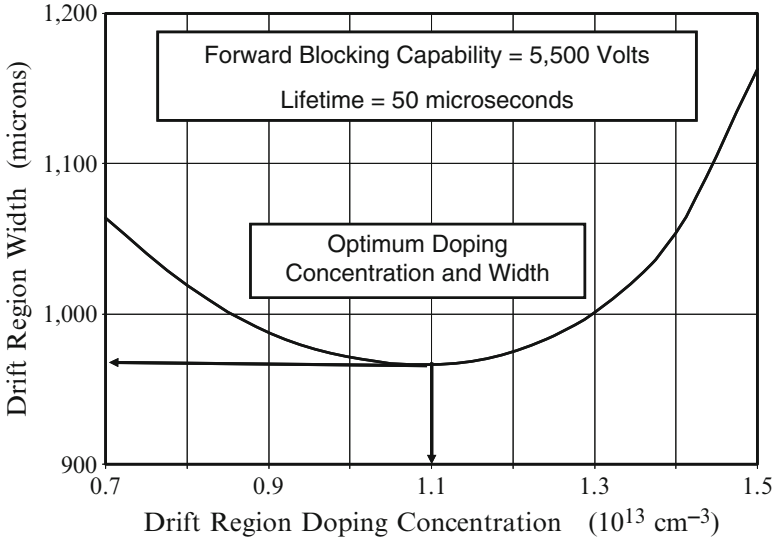

Fig. 2.7 Optimum width and doping concentration of the drift region for the 5,000-V power thyristor structure

Consider the case of a power thyristor that must have a reverse breakdown voltage of 5,500 V to achieve a blocking voltage rating of 5,000 V. In the case of avalanche breakdown, there is a unique value of 1.62×10^{13} cm^{-3} for the drift region doping concentration to obtain this blocking voltage. However, in the case of open-base transistor breakdown, many combinations of the drift region doping concentration and width can be used to obtain this blocking voltage capability. This is illustrated in Fig. 2.6 where the open-base breakdown voltage is plotted as a function of the drift region width for three cases of the drift region doping concentration. A lifetime of 50 μs was used in the N-drift region for this analysis. It can be observed from Fig. 2.6 that the open-base breakdown voltage becomes equal to 5,500 V at a drift region width of 1,070 μm for a drift region doping concentration of 0.7×10^{13} cm^{-3}. In this case, the base transport factor becomes close to unity under breakdown conditions. When the doping concentration of drift region is increased to 1.1×10^{13} cm^{-3}, the drift region thickness is reduced to 970 μm to achieve the same open-base breakdown voltage of 5,500 V. The drift region thickness increases to 1,200 μm, if the doping concentration of drift region is

increased to 1.5 $\times$ 10^{13} cm^{-3}, to achieve the same open-base breakdown voltage of 5,500 V. In this case, the multiplication coefficient becomes large under open-base breakdown conditions. These examples demonstrate that there is an optimum drift region doping concentration to obtain a minimum drift region width to achieve an open-base breakdown voltage of 5,500 V. The location of the optimum design with a width of 970 μm and doping concentration of 1.1 $\times$ 10^{13} cm^{-3} is illustrated for this case in Fig. 2.7.

The leakage current for the thyristor is determined by the space charge generation current produced by the thermally generated carriers inside the depletion region. The space generation current is amplified by the gain of the open-base PNP transistor. Consequently:

$$J_L = \frac{J_{SCG}}{1 - \alpha_{PNP}} \tag{2.5}$$

The space charge generation current increases with increasing anode bias voltage due to the enlargement of the depletion region.

$$J_{SCG} = \frac{qW_D n_i}{\tau_{SC}} = \frac{n_i}{\tau_{SC}} \sqrt{\frac{2q\varepsilon_S V_A}{N_D}} \tag{2.6}$$

As the anode bias approaches the breakdown voltage, the multiplication factor becomes larger than unity, producing a more rapid increase in the leakage current.

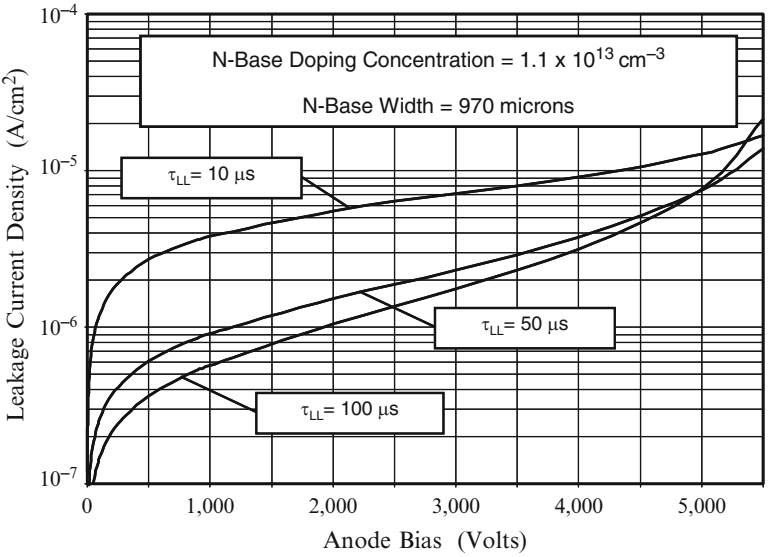

Fig. 2.8 Leakage current for the 5,000-V power thyristor structure

The leakage current density computed for the 5-kV thyristor structure by using the above analytical model is shown in Fig. 2.8. The structure had an optimized N-base doping concentration of 1.1×10^{13} cm^{-3} and optimized width of 970 μm at a lifetime of 50 μs. The impact of changing the lifetime on the leakage current is shown in the figure. The leakage current density increases when the lifetime is reduced.

Simulation Results

In order to gain insight into the physics of operation for the power thyristor under voltage blocking conditions, the results of two-dimensional numerical simulations for the optimized structure are described here. The total width of the structure, as shown by the cross section in Fig. 2.5, was 1,000 μm (area $= 1 \times 10^{-5}$ cm^{-2}) with a cathode finger width of 980 μm. The breakdown voltage obtained by using the optimized N-base region doping concentration and width from the analytical model yielded a breakdown voltage above 7,000 V. For the case of an N-drift region doping concentration of 1.5×10^{13} cm^{-3} and width of 1,070 μm, the breakdown voltage was found to be about 6,000 V. The P-base region had a Gaussian doping profile with a surface concentration of 5×10^{17} cm^{-3} and a depth of 30 μm. The N^+ cathode region had a Gaussian doping profile with a surface concentration of 1×10^{20} cm^{-3} and a depth of 10 μm. The P^+ anode region had a Gaussian doping profile with a surface concentration of 1×10^{20} cm^{-3} and a depth of 50 μm. The resulting doping profile is shown in Fig. 2.9.

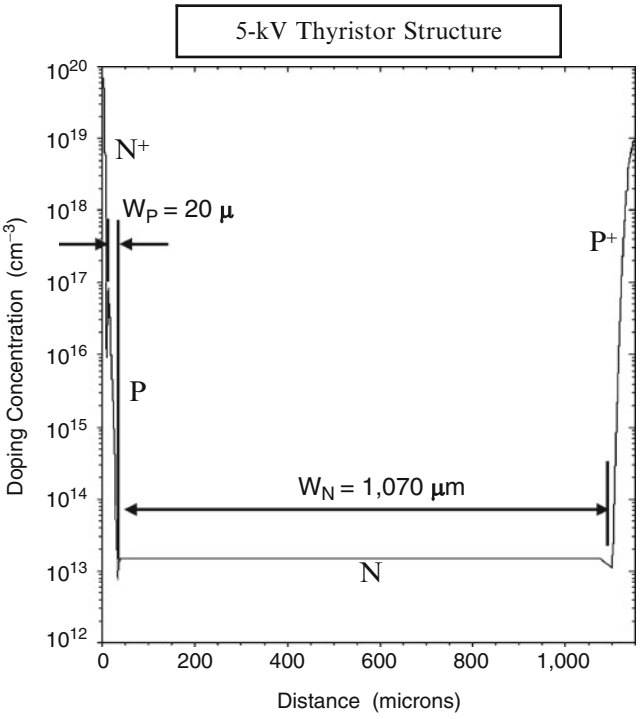

Fig. 2.9 Doping profile for the simulated 5-kV power thyristor structure

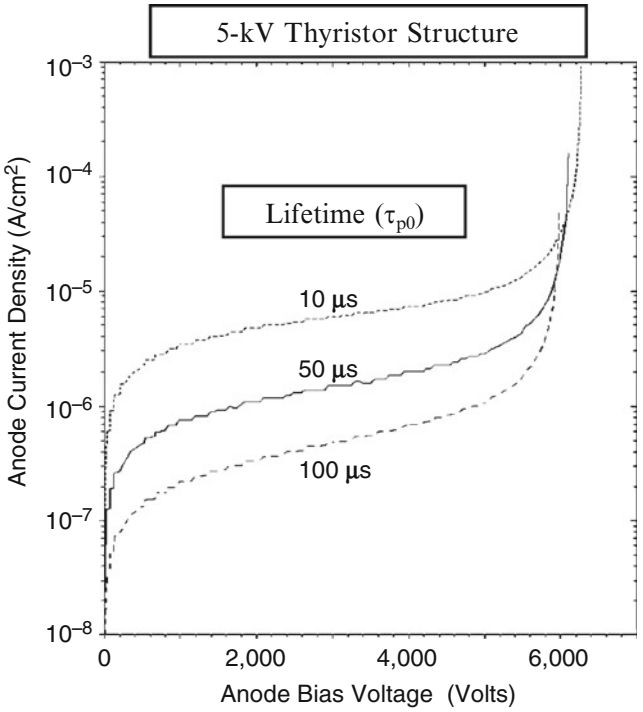

Fig. 2.10 Forward blocking characteristics for the 5-kV power thyristor structure

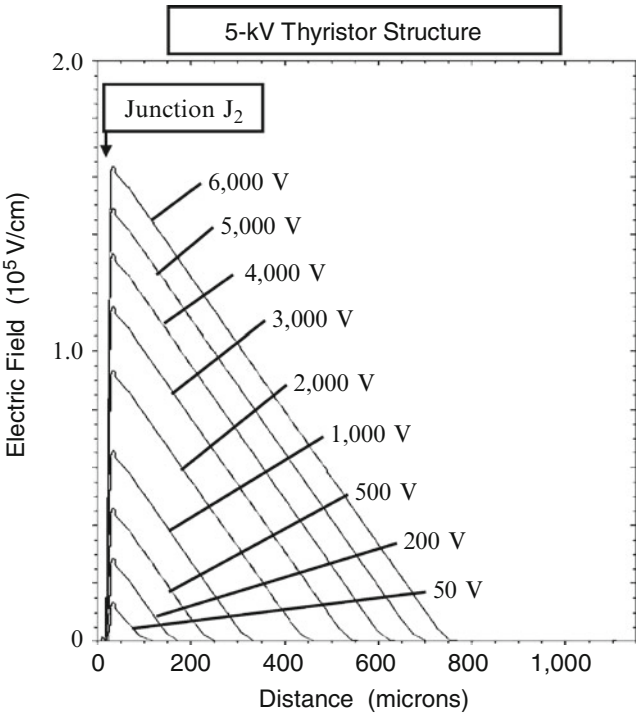

Fig. 2.11 Electric field profiles in the forward blocking mode for the 5-kV power thyristor structure

The forward blocking characteristics for the thyristor structure are shown in Fig. 2.10 for the case of various lifetime (τ_{p0}, τ_{n0}) values in the N-base region. The breakdown voltage is indicated by an abrupt increase in the anode current. At room temperature (300 K), the forward blocking voltage obtained with the simulations is about 6,000 V. The value predicted by the analytical model is smaller than this value because the analytical model does not account for the voltage being supported in the P-base region due to its graded doping profile. The leakage current density increases with decreasing lifetime as predicted by the analytical model (see Fig. 2.8) due to enhanced space charge generation.

The voltage is primarily supported in the thyristor within the N-drift region. This is illustrated in Fig. 2.11 where the electric field profiles are shown during operation in the forward blocking mode at various positive anode bias voltages. It can be observed that the P-base/N-drift junction (J_2) becomes reverse biased during the forward blocking mode with the depletion region extending toward the right-hand side with increasing anode bias. Some extension of the depletion region is observed within the P-base region due to its graded, diffused doping profile. This allows the thyristor structure to support a larger voltage than predicted by the analytical model which is based upon an abrupt junction assumption.

2.2.2 *On-State Characteristics*

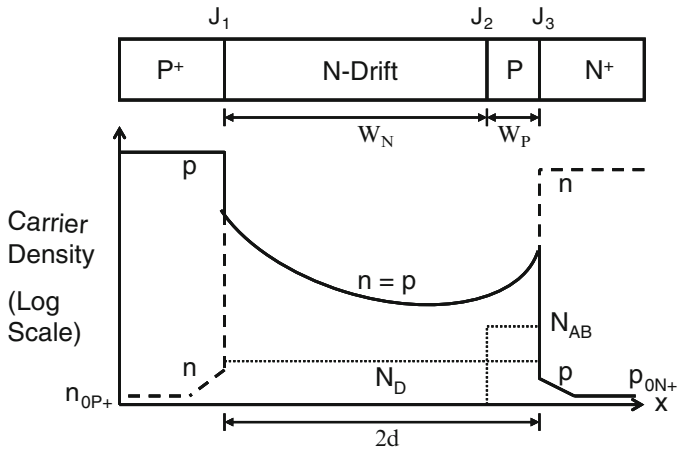

Fig. 2.12 Carrier distribution within the power thyristor structure in the on-state

One of the attributes of the thyristor structure is its excellent forward conduction characteristic even when designed to support large voltage levels. The thyristor structure can be triggered from the forward blocking mode at the anode supply voltage (V_{AS}) into the forward conduction mode by the application of a small gate current to initiate the turn-on process [1]. This gate current serves to increase the current gain of the N-P-N transistor, despite the presence of cathode shorts,

until the combined gain of the integral N-P-N and P-N-P transistors within the thyristor structure is sufficient to sustain its regenerative action. The thyristor then operates in its on-state with a forward conduction characteristic similar to that observed for a P-i-N rectifier. In the on-state, strong conductivity modulation of the N-drift region occurs due to high level injection of holes, allowing the thyristor to carry high current levels with a low on-state voltage drop.

The power thyristor can be treated as a P-i-N rectifier for analysis of its forward conduction characteristics. In this case, it is assumed that the junction J_2 is strongly forward biased resulting in high level injection in not only the N-base region but also the P-base region as illustrated in Fig. 2.12. The thyristor can then be regarded as a P-i-N rectifier between the P^+ anode and N^+ cathode regions. In this context, the N^+ cathode region is referred to as a *remote emitter* because it provides electrons to the N-base region through the intervening P-base region.

The electron and hole concentrations within the N-base and P-base regions take a catenary distribution in accordance with the analysis for the P-i-N rectifier in the textbook:

$$n(x) = p(x) = \frac{\tau_{HL} J_A}{2qL_a}\left[\frac{\cosh(x/L_a)}{\sinh(d/L_a)} - \frac{\sinh(x/L_a)}{2\cosh(d/L_a)}\right] \tag{2.7}$$

The distance "d" for the thyristor structure is given by:

$$d = \frac{W_N + W_P}{2} \tag{2.8}$$

as indicated in the figure. A minimum on-state voltage drop occurs for the thyristor structure when the ambipolar diffusion length (L_a) is equal to the distance "d" (see textbook analysis for the P-i-N rectifier in Chap. 5).

The on-state i–v characteristic for the thyristor in the high level injection regime of operation is given by [1]:

$$V_{ON} = \frac{2kT}{q}\ln\left[\frac{J_T d}{2qD_a n_i F(d/L_a)}\right] \tag{2.9}$$

where

$$F\left(\frac{d}{L_a}\right) = \frac{(d/L_a)\tanh(d/L_a)}{\sqrt{1 - 0.25\tanh^4(d/L_a)}} e^{-\frac{qV_M}{2kT}} \tag{2.10}$$

The i-region (or middle-region) voltage drop can be computed using the following approximations. For d/L_a ratios of up to 2, an asymptote A given by:

$$V_M = \frac{2kT}{q}\left(\frac{d}{L_a}\right)^2 \tag{2.11}$$

provides a good fit. For d/L_a ratios of greater than 2, an asymptote B given by:

$$V_M = \frac{3\pi kT}{8q} e^{(d/L_a)} \tag{2.12}$$

provides a good fit.

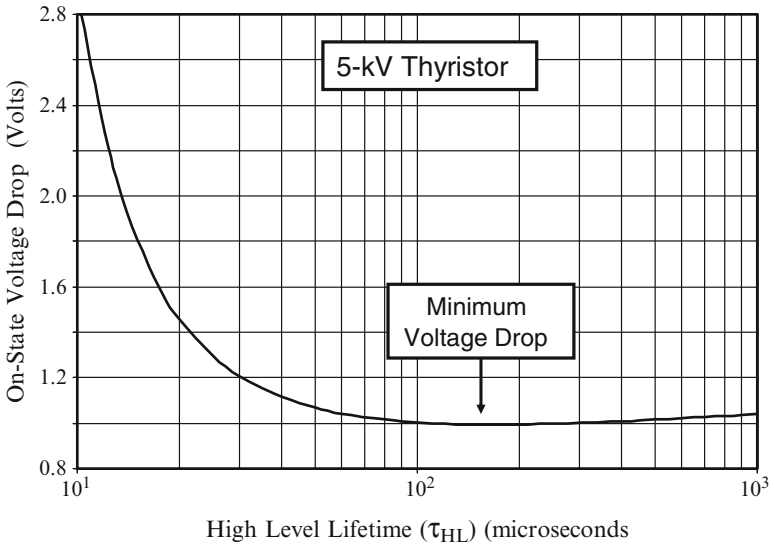

Fig. 2.13 On-state voltage drop for the 5-kV power thyristor structure

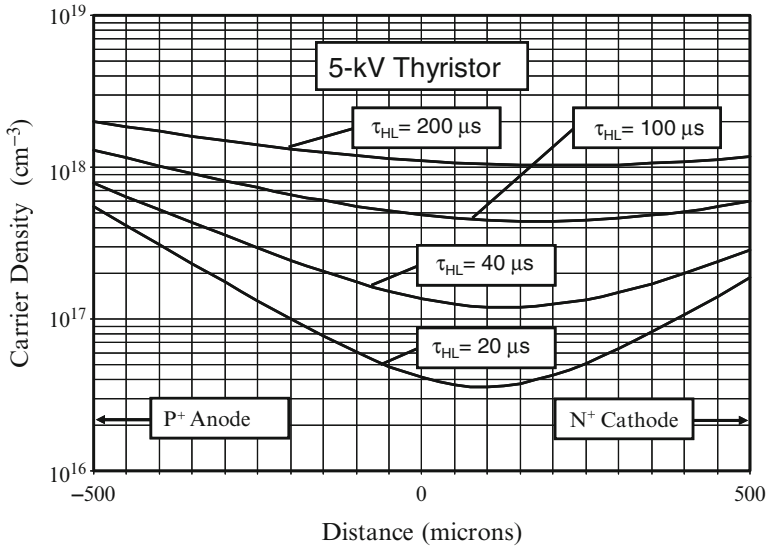

Fig. 2.14 Carrier distribution in the 5-kV power thyristor structure with middle region recombination dominant

The on-state voltage drop (at an on-state current density of 100 A/cm^2) computed for the 5-kV power thyristor structure by using Eq. 2.9 is provided in Fig. 2.13 for various values for the high-level lifetime in the drift region. This thyristor structure had the optimized N-base region width of 970 μm and a P-base width of 25 μm. As expected, the on-state voltage drop has a minimum value when the $[d/L_a]$ value is equal to unity. The minimum on-state voltage drop is found to be 0.993 V at a high-level lifetime of 160 μs.

The carrier distribution in the 5-kV thyristor structure as predicted by the analytical model based upon Eq. 2.7 is provided in Fig. 2.14 for various high-level lifetime values. As the lifetime is reduced, the injected carrier density in the drift region becomes smaller. The carrier density predicted by the analytical model is larger than in actual devices because the model is based upon assuming that recombination occurs only in the drift region. In actual devices, recombination also occurs in the end region of the device as discussed in Sect. 5.1.4 of the textbook [1]. End-region recombination reduces the injected carrier density in the drift region producing an increase in the on-state voltage drop as well.

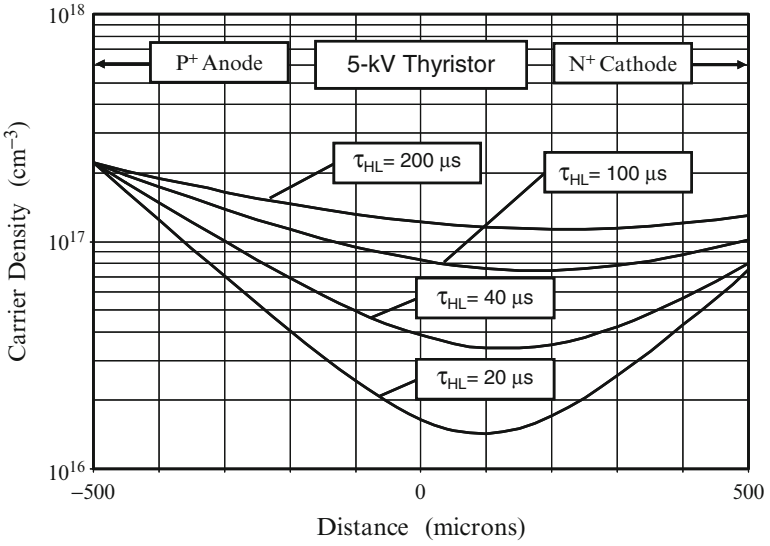

Fig. 2.15 Carrier distribution in the 5-kV power thyristor structure with end-region recombination dominant

When the lifetime in the drift region is large, end-region recombination begins to take a dominant role. Due to the high doping concentrations in the end regions, the injected minority carrier density in these regions is well below the majority carrier density even during operation at very high on-state current densities. The current corresponding to the end regions can therefore be analyzed using low-level injection theory under the assumption of a uniform doping concentration

in these regions [1]. The current flow through the device in the on-state under these conditions is described by:

$$J_{P+} = J_{SP+}\left[\frac{n(-d)}{n_{ieP+}}\right]^2 \tag{2.13}$$

for the P^+ anode region and:

$$J_{N+} = J_{SN+}\left[\frac{n(+d)}{n_{ieN+}}\right]^2 \tag{2.14}$$

for the N^+ cathode region. In these equations, n_{ieP+} and n_{ieN+} are the effective intrinsic carrier concentrations in the P^+ and N^+ end regions including the influence of band-gap narrowing. From these equations, it can be concluded that the carrier concentration in the drift region will increase as the square root of the current density if the end-region recombination becomes dominant. Under these circumstances, the middle region voltage drop is no longer independent of the current density resulting in an increase in the total on-state voltage drop.

When end-region recombination is dominant, the electron and hole concentrations within the N-base and P-base regions take a catenary distribution with a smaller concentration at the boundaries as given by Eqs. 2.13 and 2.14:

$$n(x) = p(x) = K_E\left[\frac{\cosh(x/L_a)}{\sinh(d/L_a)} - \frac{\sinh(x/L_a)}{2\cosh(d/L_a)}\right] \tag{2.15}$$

The constant K_E can be obtained by using Eq. 2.13 with $x = -d$ in the above equation. The results obtained by using this approach are shown in Fig. 2.15 for the case of various values of lifetime. A saturation current density of 4×10^{13} A/cm^2 was utilized for the plots. It can be observed that the carrier concentration is reduced by an order of magnitude when compared with the plots in Fig. 2.14.

Simulation Results

The results of two-dimensional numerical simulations for the 5-kV silicon thyristor structure are described here. The total width of the structure, as shown by the cross section in Fig. 2.5, was 1,000 μm (area = 1×10^{-5} cm^{-2}) with a cathode finger width of 980 μm. The N-base region had an optimized doping concentration of 1.5×10^{13} cm^{-3} and width of 1,070 μm. The on-state characteristics were obtained by using a gate drive current of 2×10^{-8} A/μm using various values for the lifetime in the drift region. The characteristics obtained from the numerical simulations are shown in Fig. 2.16. The small anode current observed at anode biases below 0.5 V is associated with the gate drive current. It can be observed that the on-state voltage drop increases as expected with reduction of the lifetime (τ_{p0}, τ_{n0}) indicated in the figure. The on-state voltage drop at a lifetime value of 50 μs is found to be 1.758 V at an on-state current density of 100 A/cm^2. This value is much larger than predicted by the analytical model because it does not account for recombination in the end regions.

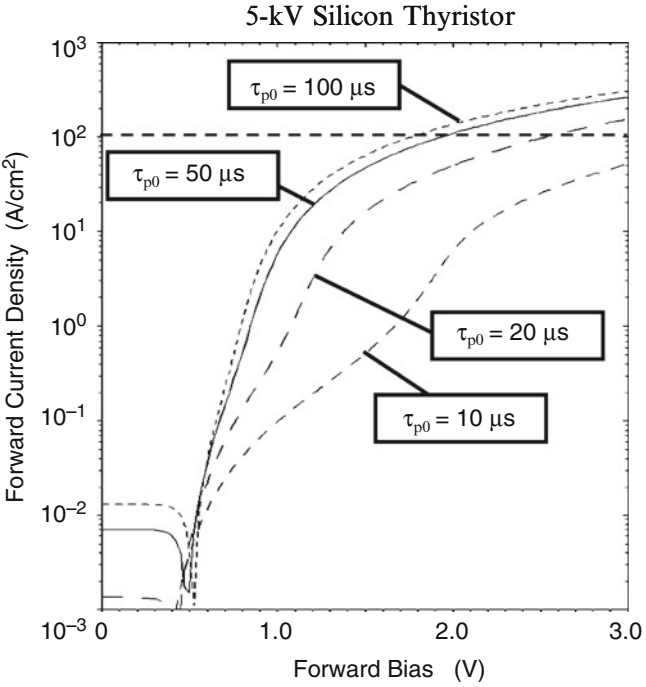

Fig. 2.16 On-state characteristics of the 5-kV power thyristor structure

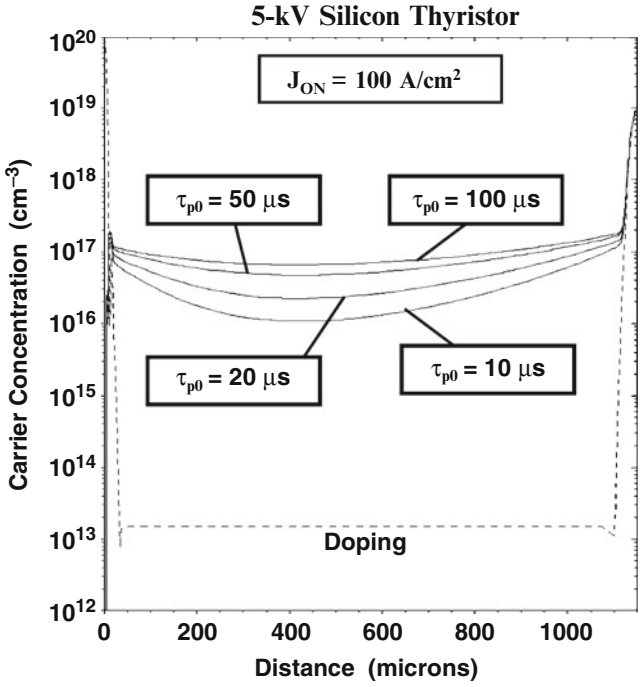

Fig. 2.17 On-state carrier distribution in the 5-kV power thyristor structure

The low on-state voltage drop for the 5-kV thyristor structure is due to the large number of carriers injected into the drift region producing a drastic reduction of its resistance. This is illustrated in Fig. 2.17 where the injected carrier density is shown for four cases of the lifetime (τ_{p0}, τ_{n0}) in the drift region of the thyristor structure. It can be observed that the injected carrier density is four orders of magnitude larger than the doping concentration for the case of a lifetime of 100 μs. The injected carrier density is reduced by an order of magnitude in the middle of the drift region when the lifetime is reduced to 10 μs. The predictions of the analytical model (see Fig. 2.14) have the same general characteristics but the injected carrier density is much smaller in the numerical simulations when compared with the analytical model that neglects the end-region recombination. When the end-region recombination is taken into account, the carrier densities predicted by the analytical model (see Fig. 2.15) are similar to those observed in the numerical simulations.

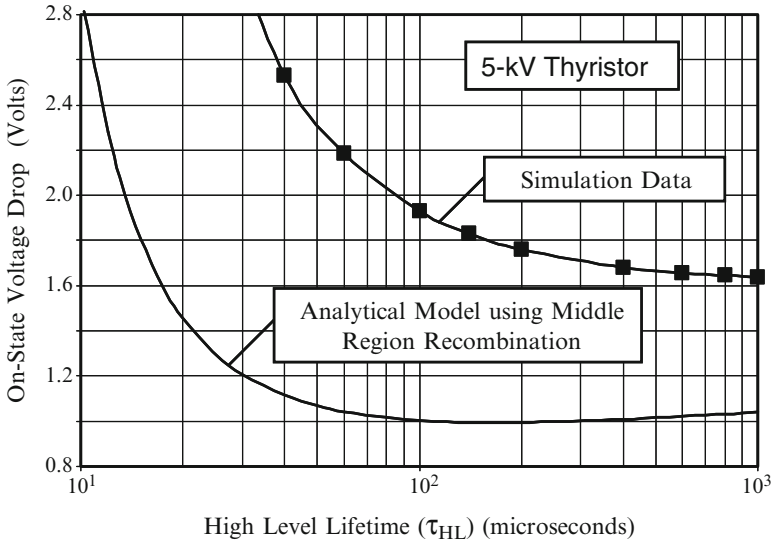

Fig. 2.18 On-state voltage drop for the 5-kV power thyristor structure obtained using numerical simulations

The reduction of the injected carrier density in the middle region with smaller lifetime leads to an increase in the on-state voltage drop. The on-state voltage drop for the 5-kV thyristor obtained using numerical simulations can be compared with that obtained using the analytical model without end-region recombination in Fig. 2.18. The on-state voltage drop obtained using numerical simulations is much larger than that predicted by the analytical model based upon middle-region recombination. Further, the minimum on-state voltage drop occurs at a significantly larger value for the lifetime in the drift region. It can be concluded that the analytical model is very optimistic and not reliable for predicting the on-state voltage drop, indicating that the impact of end-region recombination is very important for the silicon 5-kV thyristor structure.

2.2.3 Turn-On

The thyristor can be triggered from the forward blocking mode to the on-state by the application of a gate drive current. The gate drive current flows from the gate terminal to the first row of cathode shorts. The voltage drop in the P-base region due to the gate current flow forward biases the N^+ emitter/P-base junction (J_3) at the edge of the cathode closest to the gate terminal producing the injection of electrons from the cathode region. This does not immediately produce anode current flow. The injected electrons diffuse through the P-base region in a finite time interval referred to as the *base transit time*. Once the electrons cross the P-base/N-base junction (J_2), they immediately promote the injection of holes from the P^+ anode/N-base junction (J_1) in order to preserve charge neutrality in the N-base region. The injection of carriers at the P^+ anode/N-base junction initiates current flow through the device. Consequently, the anode current begins to flow after a *delay-time* interval, which is equal to the transit time for the N-P-N transistor. The delay time is typically 50 ns in duration.

After injection from the P^+ anode/N-base junction, the holes diffuse through the N-base region until they are collected at the P-base/N-base junction (J_2). The base transit time for the N-base region is a strong function of the initial anode bias voltage before turning on the thyristor [1]. The transit time can be limited by the diffusion of holes in the neutral region under the assumption that the applied anode bias is supported across only the depletion region. During the turn-on process, a high concentration of holes are injected into the N-drift region from the P^+ anode region and a high concentration of electrons are injected into the N-drift region from the N^+ cathode region (remote emitter). The depletion region cannot be sustained under these conditions and the anode voltage is distributed throughout the N-base region. The transit time for the holes is then given by [1]:

$$t_{t,PNP} = \frac{W_N}{v_P} = \frac{W_N^2}{\mu_P V_A} \tag{2.16}$$

which is much smaller than the transit time determined by the diffusion process.

An analytical model for the increase in the anode current during the turn-on transient for a one-dimensional thyristor structure was derived based upon charge control principles discussed in the textbook [1]. This analysis takes into consideration the internal feedback mechanism between the N-P-N and P-N-P transistors within the thyristor structure to determine the growth of the stored charge within the N-base region and the P-base region. Due to relatively short time for the turn-on transient when compared with the lifetime, the recombination within the N-base region and P-base region can be assumed to be negligible during this analysis. The increase in the anode current during the turn-on process is given by:

$$J_A(t) = \frac{J_G}{\alpha_{PNP}} \left(e^{t/\sqrt{t_{t,NPN} t_{t,PNP}}} - 1 \right) \tag{2.17}$$

Based upon this equation, it can be concluded that the anode current will grow exponentially with time after the delay phase. The time constant for the rise in anode current is observed to be the geometric mean of the transit times for the N-P-N and P-N-P transistors.

The *rise-time* is defined as the time taken for the anode current density to increase to the on-state value. Using Eq. 2.17, the rise-time can be obtained:

$$t_R = \sqrt{t_{t,NPN} \cdot t_{t,PNP}} \ln\left(\frac{\alpha_{PNP} J_{A,SS}}{J_G} + 1\right) \tag{2.18}$$

where $J_{A,SS}$ is the steady-state (on-state) anode current density. The rise-time is determined by the transit times for the internal N-P-N and P-N-P transistors within the thyristor structure.

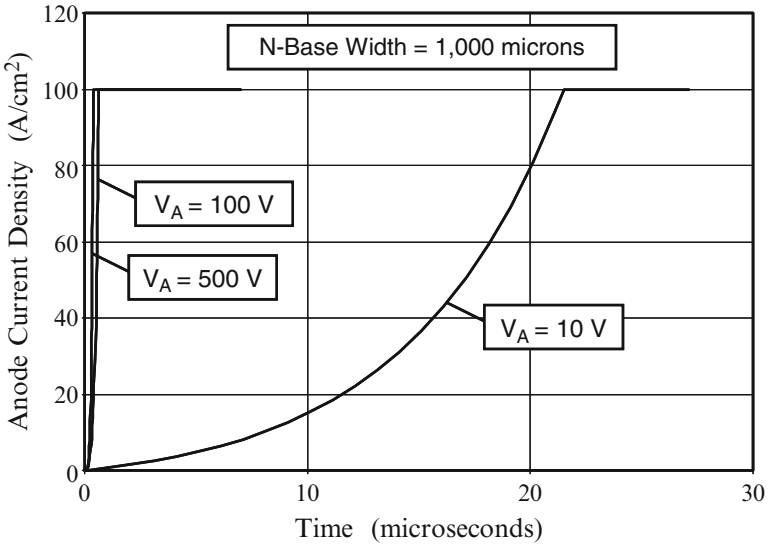

Fig. 2.19 Turn-on transient for a one-dimensional 5-kV thyristor

The rise in the anode current with time is shown in Fig. 2.19 for the case of a one-dimensional thyristor structure with a P-base region width of 25 μm and an N-base region width of 1,000 μm. The transit time for the N-P-N transistor is calculated to be 120 ns. For the case of an anode bias of 10 V, the current reaches its steady-state value with a rise-time of 21 μs. However, when the anode voltage is increased to 100 V, the transit time for the P-N-P transistor is greatly reduced to 0.2 μsdue to the enhanced drift current. Consequently, the rise-time for the anode current also decreases to only 0.5 μs. A further increase in the anode voltage to 500 V produces a reduction of the rise-time to only 0.26 μs.

Simulation Results

In order to gain further insight into the physics of turn-on for the 5-kV power thyristor structure, the results of two-dimensional numerical simulations for the structure (described in the previous section) are discussed here. The total width of the structure is 1,000 μm (area $= 1 \times 10^{-5}$ cm^{-2}) with a cathode finger width of 980 μm. In order to turn on the thyristor, the gate drive current was abruptly increased from 0 to 2×10^{-6} A/μm (0.2 A/cm^2) while the anode voltage was maintained fixed with a load resistance in series with the thyristor structure.

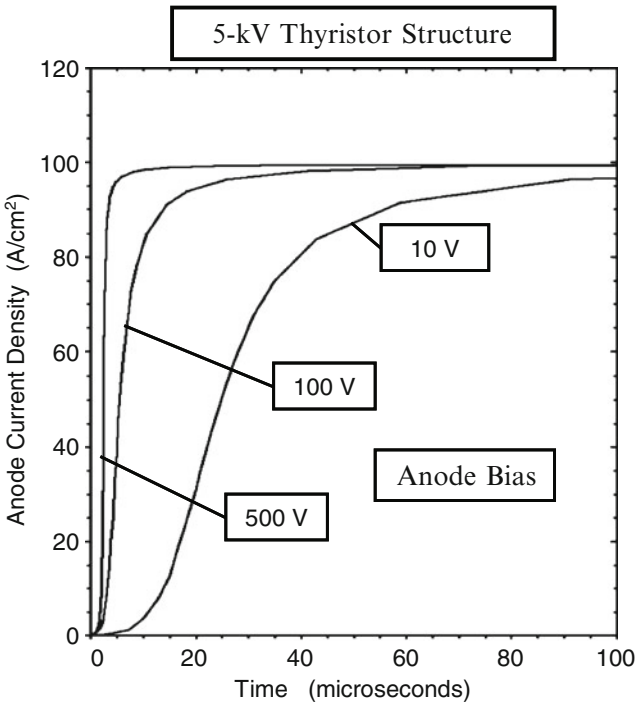

Fig. 2.20 Turn-on characteristics for the 5-kV power thyristor structure

The turn-on characteristics for the 5-kV power thyristor structure are shown in Fig. 2.20 for three values of the anode bias. In each case the load resistance was altered to obtain the same anode current density (100 A/cm^2) after the thyristor is in the on-state. In all cases, there is a short delay time of about 100 ns, which is consistent with the delay time computed by using the base transit time of the N-P-N transistor. The anode current then increases exponentially with time as described by the analytical Eq. 2.17. For the case of an anode bias of 10 V, the anode current increases exponentially for about 35 μs. This behavior is consistent with the analytical model for turn-on based upon the diffusion of carriers through the N-base region. When the anode bias is increased to 100 and 500 V, the anode

current density increases much more rapidly. This behavior is also consistent with the analytical model for turn-on based upon the drift of carriers through the N-base region. In all cases, a gradual increase in the anode current density is also observed at the end of the turn-on transient due to the current spreading across the emitter width in the two-dimensional structure used for the numerical simulations.

2.2.4 Reverse Recovery

The switching of the thyristor from the on-state to the reverse blocking state produces substantial power dissipation. The high concentration of minority carriers stored within the N-drift region due to high-level injection conditions in the on-state, must be removed before the device can support a high reverse bias voltage. When the anode voltage crosses zero, the anode current continues to flow in the reverse direction with an approximately constant rate of change or constant [di/dt] until the P^+ anode/N-base junction is able to support voltage. Once the anode voltage reaches the supply voltage, the anode current decreases to zero in an exponential manner after this junction becomes reverse biased. This behavior is similar to the reverse recovery process for the P-i-N power rectifier.

During the reverse recovery process, most of the power dissipation occurs when the anode current decays to zero after reaching the peak reverse recovery current because the anode voltage supported during this time is large (the supply voltage). The anode current waveform during the decay is described by:

$$J_A(t) = J_{PR} e^{-t/\tau_{RR}} \tag{2.19}$$

where J_{PR} is the peak reverse recovery current density and τ_{RR} is a characteristic decay time constant during the reverse recovery. The energy loss per reverse recovery transient can be obtained by integrating the instantaneous power dissipation:

$$E_{RR} = \int_0^\infty V_S J_{PR} e^{-t/\tau_{RR}} \mathrm{d}t = V_S J_{PR} \tau_{RR} \tag{2.20}$$

If switching power loss is assumed to be dominant, the maximum operating frequency for the thyristor, as limited by a power dissipation of P_D, is given by:

$$f_{Max} = \frac{P_D}{E_{RR}} \tag{2.21}$$

Simulation Results

In order to gain further insight into the physics of turn-off for the power thyristor under a constant [di/dt], the results of two-dimensional numerical simulations for the 5-kV thyristor structure (described in the previous sections) are discussed here. The total

width of the structure used for the numerical simulations was 1,000 μm (area = 1×10^{-5} cm^{-2}) with a cathode finger width of 980 μm between the gate contact and cathode short. The thyristor was switched from on-state operation at a current density of 100 A/cm^2 with a constant [d*i*/d*t*] (rate of 150 A/cm^2 in 10 μs). This reverse ramp rate was applied until the anode voltage reached −1,000 V. The anode voltage was then held constant, allowing the anode current to decay to zero.

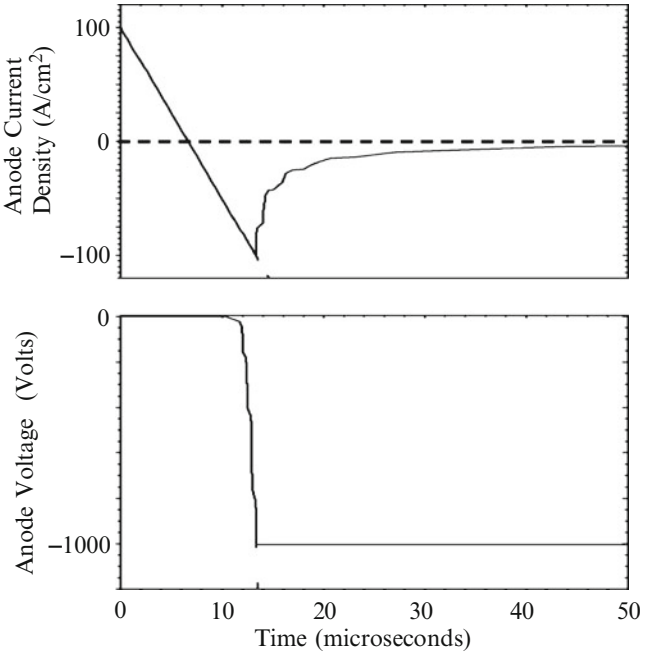

Fig. 2.21 Reverse recovery characteristics for the 5-kV thyristor structure with constant [d*i*/d*t*] applied to the anode electrode

The anode current and voltage waveforms for the thyristor are shown in Fig. 2.21. As expected, these waveforms are very similar to those exhibited by the P-i-N rectifier [1]. The anode current flows in the reverse direction until the anode voltage becomes equal to the reverse bias voltage and then decreases exponentially to zero. These waveforms confirm that the thyristor structure can be analyzed by using the reverse recovery analysis discussed in the textbook for the P-i-N rectifier. In the case of the baseline simulation structure with a lifetime (τ_{p0}, τ_{n0}) of 50 μs, the reverse recovery process requires a total time interval of about 50 μs.

2.2.5 Summary

The results of the numerical simulations discussed above indicate that the silicon 5-kV thyristor structure requires a minority carrier lifetime (τ_{p0}, τ_{n0}) of at least 50 μs to achieve a low on-state voltage drop. For such a large lifetime value,

the reverse recovery process takes over 50 μs. From the waveforms in Fig. 2.21, it can be observed that most of the power dissipation occurs during the decay of the anode current after it reaches the peak reverse recovery current density. For the conditions used during the numerical simulations, the peak reverse recovery current (J_{PR}) is found to be 100 A/cm^2 and the time constant for the reverse recovery (t_{RR}) is found to be 3.25 μs. Using a power supply voltage of 1,000 V, the energy loss per switching event is found to be 0.325 J/cm^2 by using Eq. 2.20. If the maximum power dissipation due to switching is limited to 100 W/cm^2, the maximum operating frequency for the 5-kV thyristor is then found to be 300 Hz. This demonstrates that the 5-kV silicon thyristor cannot be operated at high frequencies.

2.3 10,000-V Silicon Thyristor

The design and characteristics of the silicon 10-kV symmetric blocking thyristor structure are discussed in this section. The design parameters for the N-base region required to achieve this blocking voltage are first analyzed. Using the optimum N-base width, the blocking characteristics for the device are then obtained as a function of the lifetime in the drift region. The on-state characteristics for the device are obtained for various lifetime values as well. The switching behavior of the thyristor structure is obtained by observation of the turn-on process and the reverse recovery process.

2.3.1 Blocking Characteristics

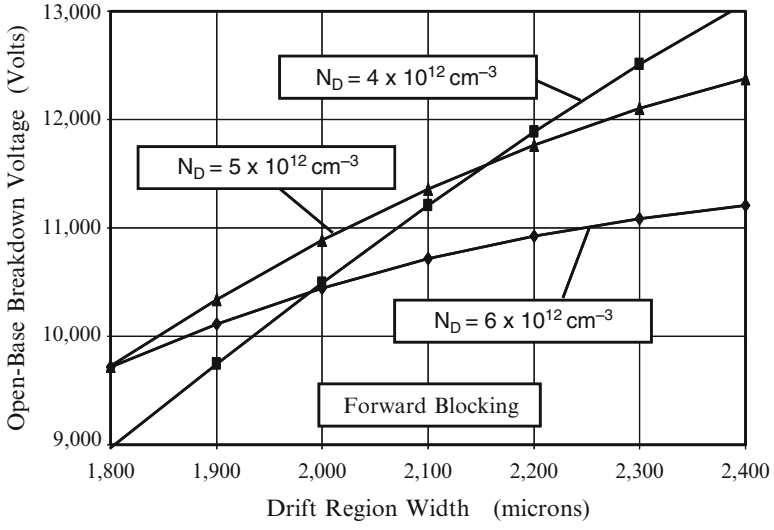

Fig. 2.22 Open-base breakdown voltage for the 10-kV power thyristor structure

The physics for blocking voltages for the 10-kV silicon symmetric blocking thyristor is identical to that for the 5-kV device described in the previous section. The open-base transistor breakdown condition is given by Eq. 2.1. Consider the case of a power thyristor that must have a reverse breakdown voltage of 11,000 V to achieve a blocking voltage rating of 10,000 V. In the case of avalanche breakdown, there is a unique value of 6.45×10^{12} cm^{-3} for the drift region doping concentration to obtain this blocking voltage. However, in the case of open-base transistor breakdown, many combinations of the drift region doping concentration and width can be used to obtain this blocking voltage capability. This is illustrated in Fig. 2.22 where the open-base breakdown voltage is plotted as a function of the drift region width for three cases of the drift region doping concentration. A lifetime of 100 μs was used in the N-drift region for this analysis. It can be observed from Fig. 2.22 that the open-base breakdown voltage becomes equal to 11,000 V at a drift region width of 2,070 μm for a drift region doping concentration of 4×10^{12} cm^{-3}. In this case, the base transport factor becomes close to unity under breakdown conditions. When the doping concentration of drift region is increased to 5×10^{12} cm^{-3}, the drift region thickness is reduced to 2,020 μm to achieve the same open-base breakdown voltage of 11,000 V. The drift region thickness increases to 2,240 μm, if the doping concentration of drift region is increased to 6×10^{12} cm^{-3}, to achieve the same open-base breakdown voltage of 11,000 V. In this case, the multiplication coefficient becomes large under open-base breakdown conditions. These examples demonstrate that there is an optimum drift region doping concentration to obtain a minimum drift region width to achieve an open-base breakdown voltage of 11,000 V. The location of the optimum design with a width of 2,020 μm and doping concentration of 4.7×10^{12} cm^{-3} is illustrated for this case in Fig. 2.23.

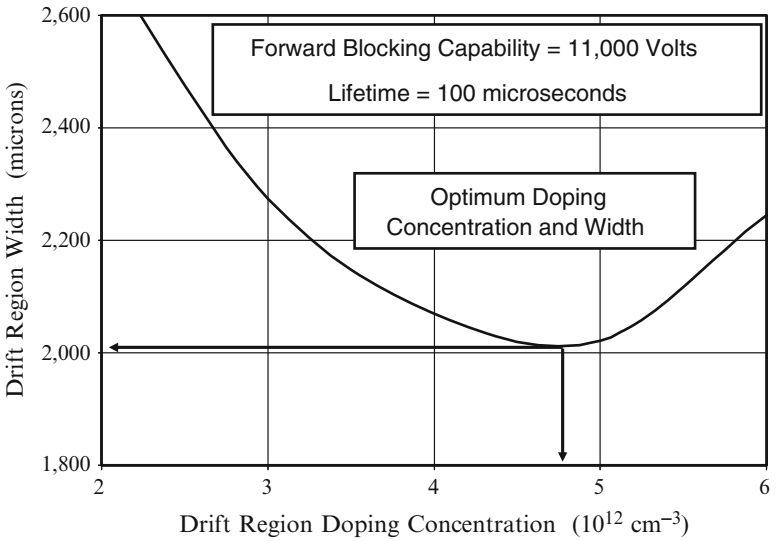

Fig. 2.23 Optimum width and doping concentration of the drift region for the 10-kV power thyristor structure

Simulation Results

In order to gain insight into the physics of operation for the 10-kV silicon power thyristor under voltage blocking conditions, the results of two-dimensional numerical simulations for the optimized structure are described here. The total width of the structure, as shown by the cross section in Fig. 2.5, was 1,000 μm (area = 1×10^{-5} cm^{-2}) with a cathode finger width of 980 μm. The P-base region had a Gaussian doping profile with a surface concentration of 5×10^{17} cm^{-3} and a depth of 30 μm. The N^+ cathode region had a Gaussian doping profile with a surface concentration of 1×10^{20} cm^{-3} and a depth of 10 μm. The P^+ anode region had a Gaussian doping profile with a surface concentration of 1×10^{20} cm^{-3} and a depth of 50 μm. An optimum N-drift region doping concentration of 5×10^{12} cm^{-3} and width of 2,000 μm was used for the baseline device structure. The doping profile is similar to that shown in Fig. 2.9.

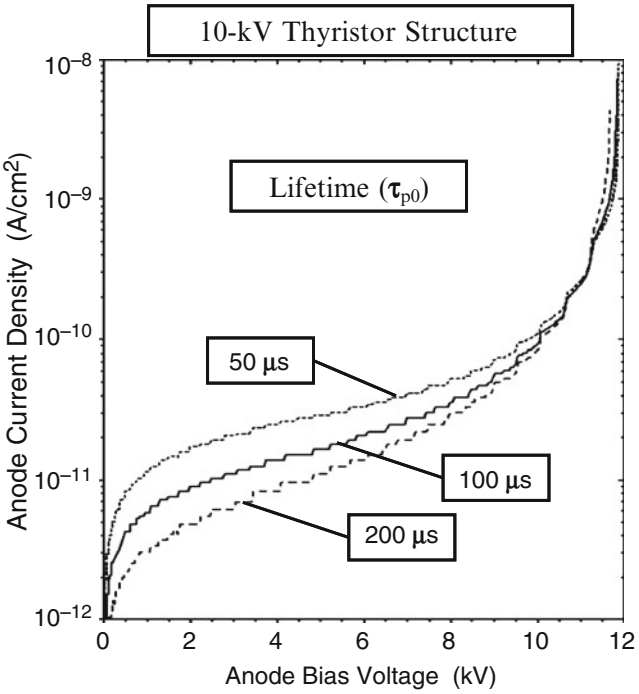

Fig. 2.24 Forward blocking characteristics for the 10-kV power thyristor structure

The forward blocking characteristics for the thyristor structure are shown in Fig. 2.24 for the case of various lifetime (τ_{p0}, τ_{n0}) values in the N-base region. The breakdown voltage is indicated by an abrupt increase in the anode current. At room temperature (300 K), the forward blocking voltage obtained with the simulations is about 11,000 V in agreement with the value predicted by the analytical model. The leakage current density increases with decreasing lifetime as predicted by the analytical model due to enhanced space charge generation.

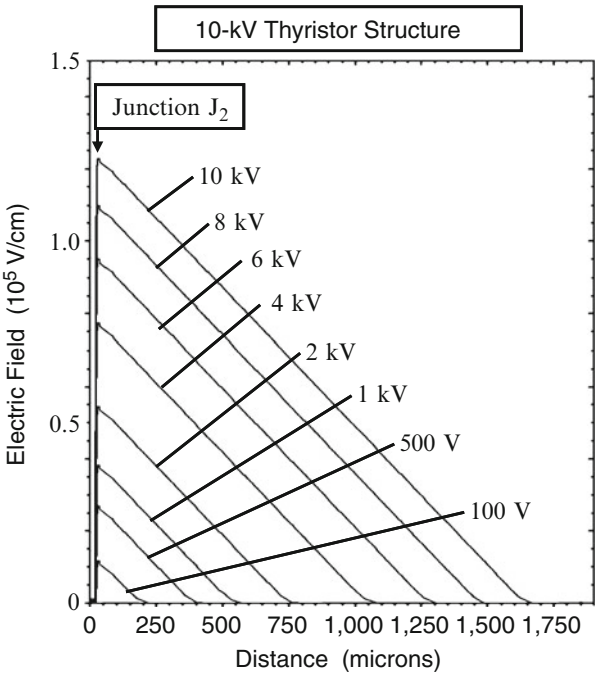

Fig. 2.25 Electric field profiles in the forward blocking mode for the 5-kV power thyristor structure

The voltage is primarily supported in the 10-kV thyristor structure within the N-drift region. This is illustrated in Fig. 2.25 where the electric field profiles are shown during operation in the forward blocking mode at various positive anode bias voltages. It can be observed that the P-base/N-drift junction (J_2) becomes reverse biased during the forward blocking mode, with the depletion region extending toward the right-hand side with increasing anode bias. Very little extension of the depletion region is observed within the P-base region. Consequently, the 10-kV thyristor structure supports voltage that is well predicted by the analytical model which is based upon an abrupt junction assumption.

2.3.2 On-State Characteristics

The on-state *i*–*v* characteristic for the 10-kV thyristor structure is described by Eq. 2.9, with a carrier distribution described by Eq. 2.7 if middle region recombination is assumed to be dominant. The on-state voltage drop (at an on-state current density of 50 A/cm^2) computed for the 10-kV power thyristor structure by using Eq. 2.9 is provided in Fig. 2.26 for various values for the high-level lifetime in the drift region. This thyristor structure had the optimized N-base region width of 2,000 μm and a P-base width of 25 μm. As expected, the on-state voltage drop has a minimum value when the $[d/L_a]$ value is equal to unity. The minimum on-state voltage drop is found to be 1.03 V at a high-level lifetime of 500–1,000 μs.

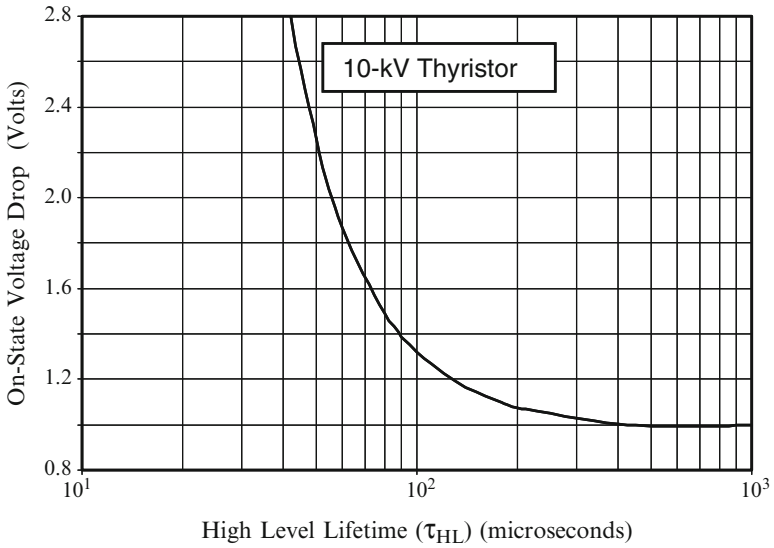

Fig. 2.26 On-state voltage drop for the 10-kV power thyristor structure

Simulation Results

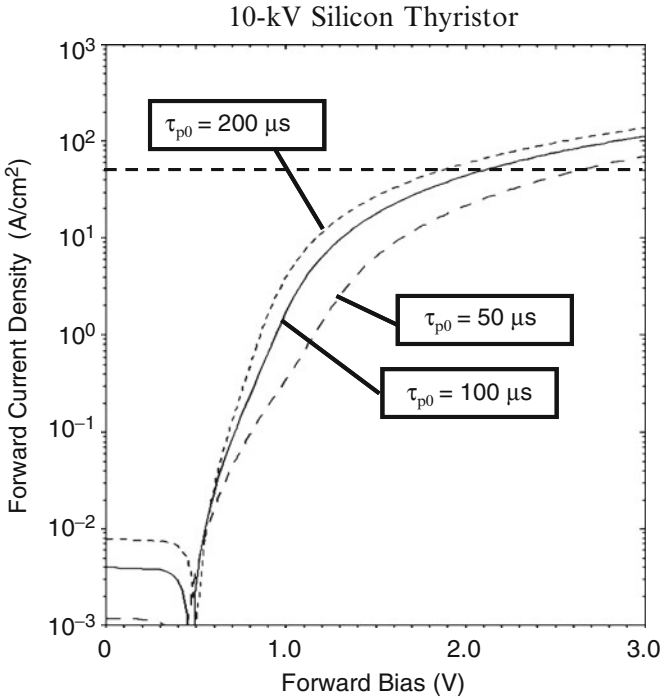

Fig. 2.27 On-state characteristics of the 10-kV power thyristor structure

The results of two-dimensional numerical simulations for the 10-kV silicon thyristor structure are described here. The total width of the structure, as shown by the cross section in Fig. 2.5, was 1,000 μm (area $= 1 \times 10^{-5}$ cm^{-2}) with a cathode finger width of 980 μm. The N-base region had an optimized doping concentration of 5×10^{12} cm^{-3} and width of 2,000 μm. The on-state characteristics were obtained by using a gate drive current of 2×10^{-8} A/μm using various values for the lifetime in the drift region. The characteristics obtained from the numerical simulations are shown in Fig. 2.27. The small anode current observed at anode biases below 0.5 V is associated with the gate drive current. It can be observed that the on-state voltage drop increases as expected with reduction of the lifetime (τ_{p0}, τ_{n0}) indicated in the figure. The on-state voltage drop at a lifetime (τ_{p0}, τ_{n0}) value of 100 μs is found to be 2.099 V at an on-state current density of 50 A/cm^2. This value is much larger than predicted by the analytical model because it does not account for recombination in the end regions.

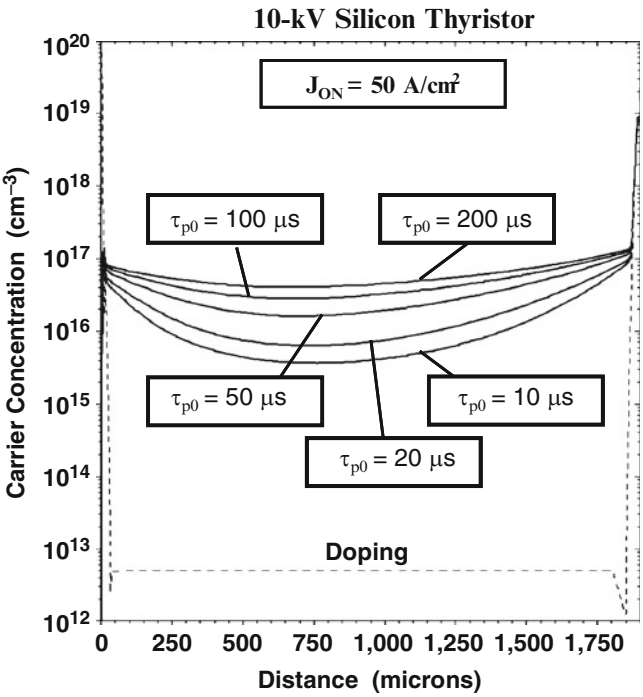

Fig. 2.28 On-state carrier distribution in the 10-kV power thyristor structure

The low on-state voltage drop for the 10-kV thyristor structure is due to the large number of carriers injected into the drift region producing a drastic reduction of its resistance. This is illustrated in Fig. 2.28 where the injected carrier density is shown for five cases of the lifetime (τ_{p0}, τ_{n0}) in the drift region of the thyristor structure. It can be observed that the injected carrier density is four orders of magnitude larger

than the doping concentration for the case of a lifetime of 200 μs. The injected carrier density is reduced by more than an order of magnitude in the middle of the drift region when the lifetime is reduced to 10 μs. As in the case of the 5-kV thyristor structure, the injected carrier density is much smaller in the numerical simulations when compared with the analytical model that neglects the end-region recombination.

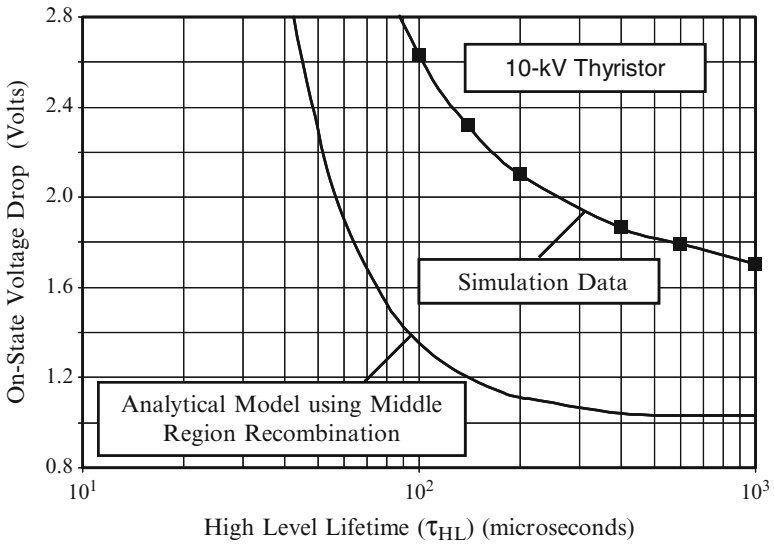

Fig. 2.29 On-state voltage drop for the 10-kV power thyristor structure obtained using numerical simulations

The reduction of the injected carrier density in the middle region with smaller lifetime leads to an increase in the on-state voltage drop. The on-state voltage drop for the 10-kV thyristor obtained using numerical simulations can be compared with that obtained using the analytical model without end-region recombination in Fig. 2.29. The on-state voltage drop obtained using the numerical simulations are much larger than those predicted by the analytical model based upon middle-region recombination. Further, the minimum on-state voltage drop occurs at a significantly larger value for the lifetime in the drift region. It can be concluded that the analytical model is very optimistic and not reliable for predicting the on-state voltage drop, indicating that the impact of end-region recombination is very important for the silicon 10-kV thyristor structure.

2.3.3 Turn-On

The 10-kV thyristor can be triggered from the forward blocking mode to the on-state by the application of a gate drive current. The analytical model for the increase in the anode current during the turn-on transient for a one-dimensional

thyristor structure was discussed in the previous section. The increase in the anode current during the turn-on process is described by Eq. 2.17. The time constant for the rise in anode current is observed to be the geometric mean of the transit times for the N-P-N and P-N-P transistors. The transit time for the holes through the N-base region of the 10-kV thyristor is much greater than in the 5-kV device because of the larger base width. This produces an increase in the rise-time for the anode current as illustrated in Fig. 2.30 for three values of the anode voltage.

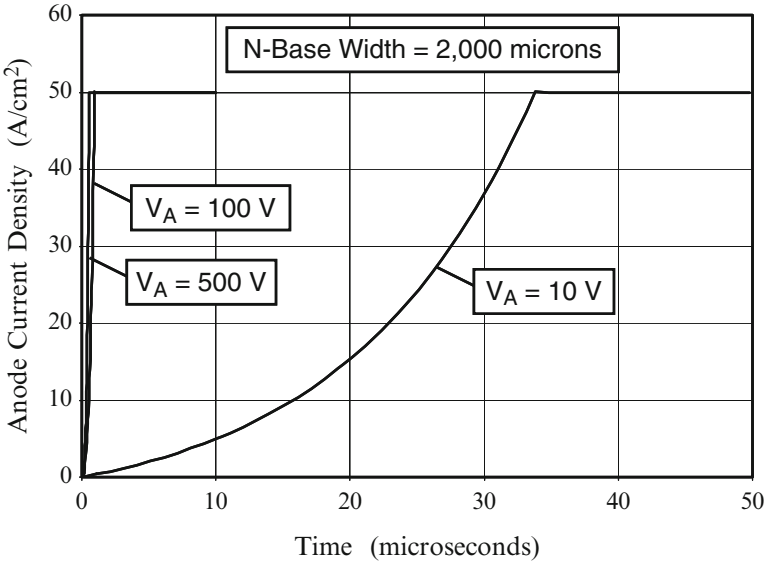

Fig. 2.30 Turn-on transient for a one-dimensional 10-kV thyristor

The rise in the anode current with time is shown in Fig. 2.30 for the case of a one-dimensional thyristor structure with a P-base region width of 25 μm and an N-base region width of 2,000 μm. The transit time for the N-P-N transistor is calculated to be 120 ns. For the case of an anode bias of 10 V, the current reaches its steady-state value with a rise-time of 34 μs. However, when the anode voltage is increased to 100 V, the transit time for the P-N-P transistor is greatly reduced due to the enhanced drift current. Consequently, the rise-time for the anode current also decreases to only 0.95 μs. A further increase in the anode voltage to 500 V produces a reduction of the rise-time to only 0.56 μs.

Simulation Results

In order to gain further insight into the physics of turn-on for the 10-kV power thyristor structure, the results of two-dimensional numerical simulations for the structure (described in the previous section) are discussed here. The total width of the structure is 1,000 μm (area $= 1 \times 10^{-5}$ cm^{-2}) with a cathode finger width of 980 μm. In order to turn on the thyristor, the gate drive current was abruptly

increased from 0 to 2×10^{-6} A/μm (0.2 A/cm^2) while the anode voltage was maintained fixed with a load resistance in series with the thyristor structure.

The turn-on characteristics for the 10-kV power thyristor structure are shown in Fig. 2.31 for three values of the anode bias. In each case the load resistance was altered to obtain the same anode current density (50 A/cm^2) after the thyristor is in the on-state. In all cases, there is a short delay time of about 100 ns, which is consistent with the delay time computed by using the base transit time of the N-P-N transistor. The anode current then increases exponentially with time as described by the analytical Eq. 2.17. For the case of an anode bias of 10 V, the anode current increases exponentially for about 80 μs. When the anode bias is increased to 100 and 500 V, the anode current density increases much more rapidly. This behavior is consistent with the analytical model for turn-on based upon the drift of carriers through the N-base region. In all cases, a gradual increase in the anode current density is also observed at the end of the turn-on transient due to the current spreading across the emitter width in the two-dimensional structure used for the numerical simulations. The analytical model describes the correct trends with increasing anode voltage but is not in quantitative agreement with the results of the numerical simulations. This is due to current spreading across the cell structure which produces a different current density than assumed for the one-dimensional analytical model.

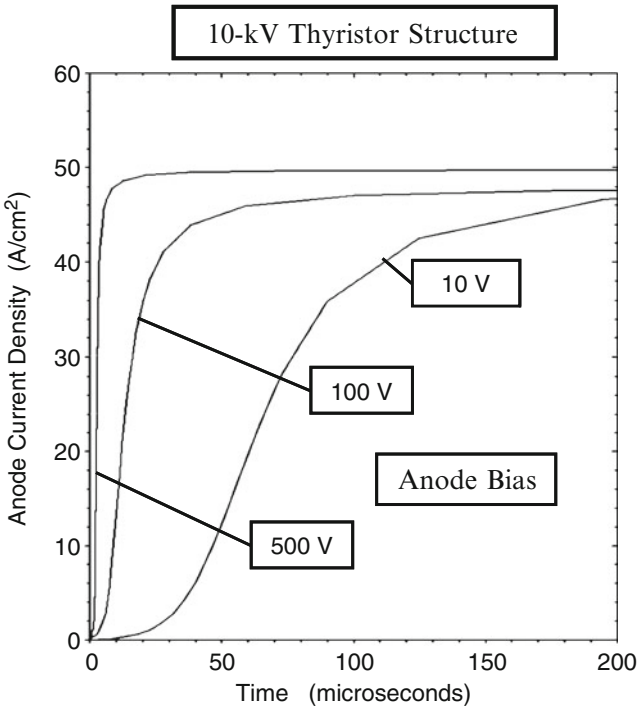

Fig. 2.31 Turn-on characteristics for the 10-kV power thyristor structure

2.3.4 *Reverse Recovery*

The reverse recovery behavior for the 10-kV thyristor structure can be expected to be similar to that previously described in Sect. 2.2.4 for the 5-kV device structure. The larger stored charge in the 10-kV device structure increases the reverse recovery current and consequently the power dissipation during this transient. This reduces the maximum operating frequency for the 10-kV device when compared with the 5-kV device.

Simulation Results

In order to gain further insight into the physics of turn-off for the power thyristor under a constant [d*i*/d*t*], the results of two-dimensional numerical simulations for the 10-kV thyristor structure (described in the previous sections) are discussed here. The total width of the structure used for the numerical simulations was 1,000 μm (area $= 1 \times 10^{-5}$ cm^{-2}) with a cathode finger width of 980 μm between the gate contact and cathode short. The thyristor was switched from on-state operation at a current density of 50 A/cm^2 with a constant [d*i*/d*t*] (rate of 75 A/cm^2 in 10 μs). This reverse ramp rate was applied until the anode voltage reached −1,000 V. The anode voltage was then held constant, allowing the anode current to decay to zero.

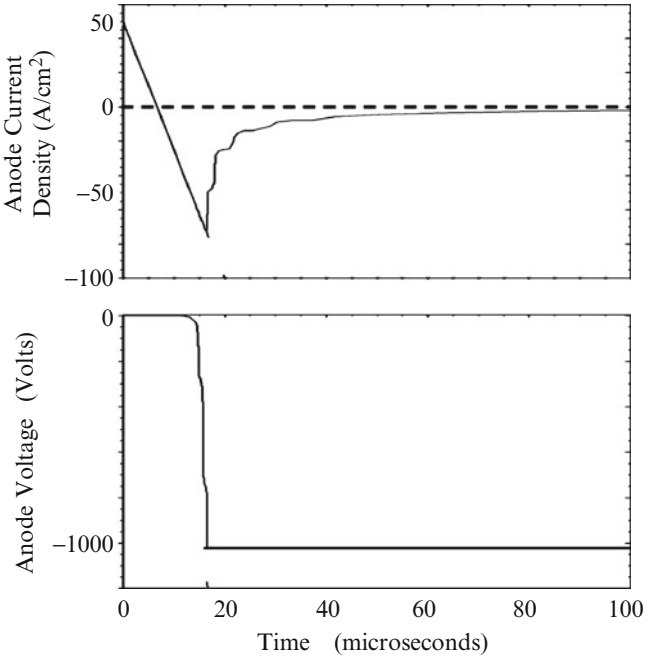

Fig. 2.32 Reverse recovery characteristics for the 10-kV thyristor structure with constant [d*i*/d*t*] applied to the anode electrode

The anode current and voltage waveforms for the thyristor are shown in Fig. 2.32. As expected, these waveforms are very similar to those exhibited by the P-i-N rectifier. The anode current flows in the reverse direction until the anode voltage becomes equal to the reverse bias voltage and then decreases exponentially to zero. These waveforms confirm that the thyristor structure can be analyzed by using the reverse recovery analysis discussed in the textbook for the P-i-N rectifier. In the case of the baseline simulation structure with a lifetime (τ_{p0}, τ_{n0}) of 100 μs, the reverse recovery process requires a total time interval of about 100 μs.

2.3.5 Summary

The results of the numerical simulations discussed above indicate that the silicon 10-kV thyristor structure requires a minority carrier lifetime (τ_{p0}, τ_{n0}) of at least 100 μs to achieve a low on-state voltage drop. For such a large lifetime value, the reverse recovery process takes over 100 μs. From the waveforms in Fig. 2.32, it can be observed that most of the power dissipation occurs during the decay of the anode current after it reaches the peak reverse recovery current density. For the conditions used during the numerical simulations, the peak reverse recovery current (J_{PR}) is found to be 74 A/cm^2 and the time constant for the reverse recovery (t_{RR}) is found to be 6.75 μs. Using a power supply voltage of 1,000 V, the energy loss per switching event is found to be 0.50 J/cm^2 by using Eq. 2.20. If the maximum power dissipation due to switching is limited to 100 W/cm^2, the maximum operating frequency for the 10-kV thyristor is then found to be 200 Hz. This demonstrates that the 10-kV silicon thyristor cannot be operated at frequencies as high as the 5-kV device.

2.4 Conclusions

The design and characteristics of the 5-kV and 10-kV silicon thyristor structures have been analyzed in this chapter. Such high voltage ratings require extremely high resistivity silicon wafers with relatively large thickness. The large thickness of the drift region limits the ability to reduce the lifetime in the drift region to improve the switching speed as determined by the reverse recovery process. Typical silicon devices are found to be limited to an operating frequency of less than 300 Hz for the 5-kV device and 200 Hz for the 10-kV device.

References

1. B.J. Baliga, “Fundamentals of Power Semiconductor Devices”, Springer-Science, 2008.
2. I.M. Mackintosh, “The Electrical Characteristics of Silicon p-n-p-n Triodes”, Proc. IRE, Vol. 46, pp. 1229, 1958.
3. R.W. Aldrich and N. Holonyak, “Multiterminal p-n-p-n Switches”, Proc. IRE, Vol. 46, pp. 1236, 1958.
4. A. Herlet, “The Maximum Blocking Capability of Silicon Thyristors”, Solid State Electronics, Vol. 8, pp. 655–671, 1965.

http://www.springer.com/978-1-4614-0268-8

Advanced High Voltage Power Device Concepts
Baliga, B.J.
2012, XVI, 568 p., Hardcover
ISBN: 978-1-4614-0268-8